

Magnetic structure of isospin-asymmetric QCD matter in neutron stars

G. Endrődi¹

¹*Institute for Theoretical Physics, Universität Regensburg, D-93040 Regensburg, Germany*
E-mail: gergely.endrodi@physik.uni-r.de

We study QCD under the influence of background magnetic fields and isospin chemical potentials using lattice simulations. This setup exhibits a sign problem which is circumvented using a Taylor-expansion in the magnetic field. The ground state of the system in the pion condensation phase is found to exhibit a pronounced diamagnetic response. We elaborate on how this diamagnetism may contribute to the pressure balance in the inner core of strongly magnetized neutron stars. In addition we show that the onset of pion condensation shifts to larger chemical potentials due to the enhancement of the charged pion mass for growing magnetic fields. Finally, we summarize the magnetic nature of QCD matter on the temperature-isospin chemical potential phase diagram.

PACS numbers: 12.38.Gc, 12.38.Mh, 97.60.Jd

1. INTRODUCTION

The elementary degrees of freedom of the high-energy phase of Quantum Chromodynamics (QCD) are deconfined quarks and gluons. One physical environment where this deconfined phase may exist is the inner core of dense neutron stars – compact stellar objects created during the gravitational collapse of massive stars. A certain class of neutron stars (magnetars) exhibits intense magnetic fields of strengths up to 10^{14-15} G at the star surface. These extreme magnetic fields are presumably generated by a convective dynamo mechanism during the first few seconds after the collapse [1], and are believed to be responsible for the strong electromagnetic activity of the star in the form of gamma-ray and X-ray bursts [2]. Magnetic fields can induce a strong deformation of the star, leading to the radiation of gravitational waves [3]. During mergers of binary neutron star systems, magnetic fields can even be amplified drastically [4] and have a significant impact on the emitted gravitational signal [5]. Thus, an understanding of the behavior of neutron star matter in magnetic fields is desired in many respects.

While the magnetic fields at the surface of the star are typically determined using measurements of rotation periods and time derivatives thereof [6], the strength of the field in the deep interior of the star is highly uncertain. On general grounds the field B is expected to become enhanced towards the star center, see, e.g., Ref. [7]. The maximal possible strength is estimated to be $B \approx 10^{18}$ G based on the equality of the gravitational and magnetic energies [6]. These extreme values for B are in the regime where a competition between the electromagnetic and the strong forces takes place and the magnetic properties of QCD matter as a medium become important.

An additional characteristic aspect of neutron stars is the isospin asymmetry that develops in their interior through protons converting into neutrons and neutrinos via electron capture. The core is thus described by a high baryonic density accompanied by a considerable isospin density. In the grand canonical approach to statistical physics, these densities are controlled by the correspond-

ing chemical potentials. On the level of the (up and down) quark content, they are written as

$$\mu_B = 3(\mu_u + \mu_d)/2, \quad \mu_I = (\mu_u - \mu_d)/2. \quad (1)$$

To understand the structure of the dense and strongly magnetized inner core, an investigation of the combined effect of μ_f ($f = u, d$ labels the quark flavors) and B on the ground state of QCD matter is necessary. In the strongly interacting regime this is only possible using non-perturbative approaches like lattice simulations.

To leading order in B , the magnetic response of the system is characterized by the magnetic susceptibility,

$$\langle \chi \rangle = -\frac{1}{V} \left. \frac{\partial^2 \mathcal{F}}{\partial (eB)^2} \right|_{B=0}, \quad (2)$$

defined in terms of the free energy $\mathcal{F} = -T \log \mathcal{Z}$ of the system (V denotes the three-dimensional volume, T the temperature and \mathcal{Z} the partition function). Here we considered the magnetic field in units of the elementary charge $e > 0$. Note that the first derivative of \mathcal{F} at $B = 0$ vanishes due to parity symmetry. The sign of χ distinguishes between paramagnetism ($\chi > 0$) and diamagnetism ($\chi < 0$).

In this letter we calculate the magnetic susceptibility at nonzero isospin chemical potentials and discuss the structure of the $\mu_I - B - T$ phase diagram using numerical lattice QCD simulations. Our results indicate a strong diamagnetic response at high μ_I , where charged pions condense. This response is related to the superconducting nature of the pion condensate. We also present an argument suggesting that χ is less affected by the baryonic chemical potential and, thus, μ_I is the most relevant control parameter for the magnetic response of QCD at nonzero densities. In addition, we discuss the impact of the diamagnetic nature of the isospin-asymmetric state on magnetars. Assuming typical magnetic field configurations, this diamagnetism results in a considerable anisotropic force that can compete with the gravitational pressure in the core. This may have implications on, e.g., the convective processes in the interior of the star.

2. LATTICE SETUP AND OBSERVABLES

We consider QCD with two quark flavors, described by a two-component quark field $\psi = (\psi_u, \psi_d)$ and the fermion matrix

$$M = \begin{pmatrix} \not{D}(\mu_I, q_u) + m & \lambda\gamma_5 \\ -\lambda\gamma_5 & \not{D}(-\mu_I, q_d) + m \end{pmatrix} \quad (3)$$

where q_f is the electric charge of the quark of flavor f , and we assumed a degenerate mass m . Here, $\not{D} = \gamma_\nu D_\nu$ is the Dirac operator with the $SU(3) \times U(1)$ covariant derivative $D_\nu = \partial_\nu + iA_\nu + iq_f A_\nu^{\text{em}}$. The Abelian vector potential is chosen such that it generates a magnetic field in the z direction, $A_4^{\text{em}} = 0$, $\nabla \times \mathbf{A}^{\text{em}} = \mathbf{B} \parallel \hat{\mathbf{z}}$.

The term proportional to λ is inserted in Eq. (3) as a small explicit breaking to allow the observation of pion condensation, corresponding to the expectation value $\langle \pi \rangle \equiv \langle \bar{\psi}_u \gamma_5 \psi_d - \bar{\psi}_d \gamma_5 \psi_u \rangle$. This expectation value signals the spontaneous breakdown of isospin symmetry (more precisely: an $U(1)$ subgroup of the full isospin group that is left intact at $m \neq 0$ and $\mu_I \neq 0$). In a finite volume this spontaneous breaking cannot occur without a small explicit breaking. The coefficient λ will be extrapolated to zero at the end of the analysis. Incidentally, for $\mu_I \gtrsim m$ the smallest eigenvalue of the Hermitian operator $M^\dagger M$ (which is used in the simulation algorithm) equals λ^2 , such that the system becomes ill-conditioned as $\lambda \rightarrow 0$. Nevertheless, for the values necessary to perform this extrapolation (see Sec. 3) this numerical problem still turned out to be feasible.

This theory is simulated on a symmetric N^4 lattice with $N = 8$ such that the spatial volume equals $V = L^3 = (8a)^3$ with a being the lattice spacing. To allow for a cross-check of the algorithm and of the simulation code, we use the same lattice discretization as Ref. [8]: the plaquette gauge action $S_p(\beta)$ and rooted staggered quarks. The partition function is obtained via the functional integral over the gluonic links $U_\nu = \exp(iaA_\nu)$ as

$$\mathcal{Z} = \int \prod_\nu \mathcal{D}U_\nu e^{-S_p(\beta)} \det M^{1/4}. \quad (4)$$

The inverse gauge coupling is $\beta \equiv 6/g^2 = 5.2$ and the quark mass in lattice units equals $ma = 0.025$. The lattice spacing is determined using the Wilson flow [9] via the w_0 scale proposed in Ref. [10] to be $a = 0.299(2)$ fm. The linear size of the system is $L \approx 2.4$ fm. Thus, $L^{-1} \approx 80$ MeV is well below the finite temperature deconfinement transition and the system may be approximated as being at zero temperature. Through fitting the pseudoscalar propagator we get for the pion mass in lattice units $m_\pi a = 0.402(5)$, giving $m_\pi \approx 260$ MeV.

Using the γ_5 -hermiticity of the Dirac operator (for staggered quarks the role of γ_5 is played by $\eta_5 = (-1)^{n_x+n_y+n_z+n_t}$),

$$\gamma_5 \not{D}(\mu_I, q) \gamma_5 = \not{D}(-\mu_I, q)^\dagger, \quad (5)$$

one can prove that the fermionic action $S_f \propto -\log \det M$ is real and positive if the electric charges of the two flavors coincide. However, having $q_d = -2q_u = -e/3$ is essential to capture the fact that the particles excited by the isospin chemical potential are the *charged* pions. Therefore, in the presence of the magnetic field, S_f becomes complex and cannot be simulated using conventional lattice Monte-Carlo methods.

We tackle this complex action problem by simulating at $\mu_I \neq 0$ and $B = 0$ – where S_f is real and positive – and performing a (leading-order) Taylor-expansion in the magnetic field. This expansion involves the derivatives of the free energy with respect to eB – starting with χ of Eq. (2). One technical complication is that on a finite lattice with periodic boundary conditions, the magnetic flux $\Phi = eB \cdot L^2$ is quantized [11], making the derivative with respect to eB ill-defined. An advantageous strategy is to consider a modified magnetic field, for example one that is positive in one half and negative in the other half of the lattice [12], $\mathbf{B} = B \text{sign}(L/2 - x) \cdot \hat{\mathbf{z}}$. To implement this magnetic field configuration, the Abelian links $u_\nu^f = \exp(iaq_f A_\nu^{\text{em}})$ for the flavor f are chosen as [12]

$$\begin{aligned} u_y^f(n_x) &= e^{ia^2 q_f B \cdot (n_x - N/4)}, & n_x \leq N/2, \\ u_y^f(n_x) &= e^{ia^2 q_f B \cdot (3N/4 - n_x)}, & n_x > N/2, \\ u_\nu^f &= 1, & (\nu \neq y), \end{aligned} \quad (6)$$

where $n_x = x/a$ denotes the x -coordinate of the sites. The links (and, thus, also the magnetic field) satisfy periodic boundary conditions. This setup was tested to give reliable results at $\mu_I = 0$, where a direct simulation at $B \neq 0$ is also possible [13]. Nevertheless, we mention that finite volume effects may become enhanced due to the presence of the boundaries where the magnetic field changes sign, and for precision results our measurements should be repeated on larger volumes.

Since the total magnetic flux is zero, the derivative with respect to eB – being a continuous variable – can now be taken. Differentiating Eq. (4) twice, the susceptibility Eq. (2) reads

$$\langle \chi \rangle = \frac{\langle \mathcal{C}_2 \rangle}{N^4}, \quad \mathcal{C}_2 = \mathcal{C}_1^2 + \mathcal{C}_1', \quad \mathcal{C}_1 = \frac{1}{4} \text{Tr}(M^{-1} M'), \quad (7)$$

where $\langle . \rangle$ denotes the expectation value with respect to \mathcal{Z} and the prime the derivative with respect to eB . Besides the magnetic susceptibility, we also consider other observables like the chiral condensate, the pion condensate and the isospin density

$$\langle \bar{\psi} \psi \rangle = -\frac{1}{V} \frac{\partial \mathcal{F}}{\partial m}, \quad \langle \pi \rangle = -\frac{1}{V} \frac{\partial \mathcal{F}}{\partial \lambda}, \quad \langle n_I \rangle = -\frac{1}{V} \frac{\partial \mathcal{F}}{\partial \mu_I}. \quad (8)$$

The second derivative of the expectation value of either of these observables $\mathcal{O} = \bar{\psi} \psi, \pi$ or n_I can be found as

$$\left. \frac{\partial^2 \langle \mathcal{O} \rangle}{\partial (eB)^2} \right|_{B=0} = \langle \mathcal{O}'' \rangle + 2\mathcal{O}' \mathcal{C}_1 + \mathcal{O} \mathcal{C}_2 - \langle \mathcal{O} \rangle \langle \mathcal{C}_2 \rangle. \quad (9)$$

In addition we will also discuss the Polyakov loop as a measure for deconfinement,

$$P = \frac{1}{V} \sum_x \text{Tr} \exp \left[\int dt A_4(x, t) \right]. \quad (10)$$

We remark that the magnetic susceptibility contains an additive divergence at zero temperature and zero density, such that its renormalization reads

$$\langle \chi \rangle^r = \langle \chi \rangle - \langle \chi \rangle_{\mu_I=T=0}. \quad (11)$$

This renormalization is related to the electric charge and wavefunction renormalization in QED [14]. The B -dependent divergence cancels from the observables of Eqs. (8) and (10). For more details on this renormalization see, e.g., Ref. [13]. In the following, the expectation value $\langle \cdot \rangle$ is suppressed for the sake of brevity.

3. RESULTS

We begin by considering the observables of Eq. (8) at vanishing magnetic field. Fig. 1 shows the results at various values of the explicit symmetry breaking parameter λ and a linear extrapolation to $\lambda = 0$ for each μ_I . The difference to a quadratic extrapolation is used to define the systematic uncertainty, and is included in the errors shown in the plot. We observe that the $\lambda = 0$ limit of π vanishes in the low- μ_I region, whereas it increases drastically for high chemical potentials, signalling the con-

densation of pions. The onset of this condensation is predicted by chiral perturbation theory (χ PT) to occur at $\mu_I = m_\pi/2$ [16], in good agreement with the lattice data. All other observables are also insensitive to μ_I (in the $\lambda \rightarrow 0$ limit) up to this onset value. This is in general referred to as the Silver Blaze phenomenon. The chiral condensate drops sharply above $\mu_I = m_\pi/2$, while the isospin density starts to grow at the condensation threshold. We note that our results are within statistical errors consistent with those of Ref. [8], up to the fact that in Ref. [8] a different normalization convention was used. Our normalization is chosen such that the results at $\mu_I = 0$ correspond to two degenerate flavors. We note moreover that lattice discretization effects start to dominate for $a\mu_I \gtrsim 1$ (not visible in the plot): here all lattice sites become occupied and the isospin density saturates at $a^3 n_I^{\text{sat}} = 3/2$.

To perform the λ -extrapolation in a more effective manner, we consider χ PT to describe the behavior of the observables for small λ and for small μ_I [15]. This dependence involves two parameters: the pion mass and the chiral condensate at $\mu_I = \lambda = 0$, denoted by G ,

$$\bar{\psi}\psi = G \cos \alpha, \quad \pi = G \sin \alpha, \quad n_I = \frac{4mG\mu_I}{m_\pi^2} \sin^2 \alpha, \quad (12)$$

where α is the vacuum angle, determined at the extremum of \mathcal{F} by

$$\sin(\alpha - \phi) = \frac{4\mu_I^2}{m_\pi^2} \sin \alpha \cos \alpha, \quad \phi = \arctan \lambda/m. \quad (13)$$

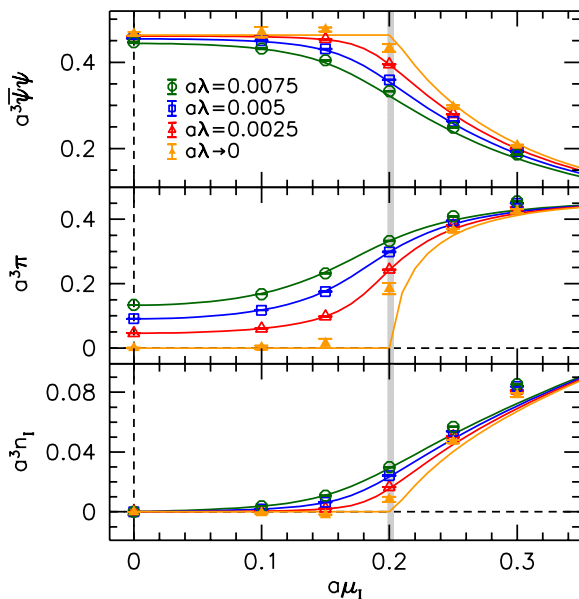


FIG. 1: Quark condensate (upper panel), pion condensate (middle panel) and isospin density (lower panel) as functions of the isospin chemical potential for various λ values (red, blue and green points), a linear fit $\lambda \rightarrow 0$ (yellow points), and a combined fit using χ PT [15] (solid lines). The onset of pion condensation at $m_\pi/2$ is indicated by the gray vertical line.

We carry out a simultaneous fit of all three observables, using data points for all values of λ , up to $a\mu_I = 0.2$. Considering the pion mass as a free parameter of the fit, we obtain $am_\pi = 0.4053(1)$, consistent with our previous determination using the pseudoscalar propagator. The latter is indicated by the gray line in the figure. For the condensate the fit gives $G = 0.4657(2)$. In fact, χ PT predicts pion condensation and chiral symmetry restoration to proceed simultaneously such that $\pi^2 + \bar{\psi}\psi^2$ remains constant. The lattice data do not support this prediction for $\mu_I \gtrsim m_\pi/2$, as π turns out to be underestimated by χ PT (this was also realized in Ref. [8]). However, below $m_\pi/2$ – where the λ -dependence is most pronounced and, thus, the extrapolation cumbersome – the χ PT prediction is in excellent agreement with the lattice data. This comparison also reveals that the linear $\lambda \rightarrow 0$ extrapolations of the lattice data using the available three λ values – with the exception of the points just at the condensation threshold – are reliable. Note that a true phase transition only appears in the thermodynamic limit, and in a finite volume the observables slightly deviate from the behavior dictated by χ PT around the onset chemical potential. As a side remark, we also mention that the structure of the chiral Lagrangian is the same for two-color QCD and for QCD with adjoint quarks. Thus, Eqs. (12) and (13) are also valid in these settings [17].

We proceed by performing a similar, linear $\lambda \rightarrow 0$ extrapolation for the renormalized magnetic susceptibility Eq. (11). Subtracting the $\mu_I = 0$ contribution at each λ turned out to be advantageous here as it makes the $\lambda \rightarrow 0$ extrapolation flatter. The results again show a Silver Blaze-type behavior up to $m_\pi/2$ and a rapid drop towards negative values beyond the onset of pion condensation (see upper panel of Fig. 2). This implies that the QCD medium at low temperatures is *diamagnetic* for $\mu_I > m_\pi/2$. The diamagnetic response may be understood qualitatively from the fact that just above $m_\pi/2$, the system can be approximated as a dilute gas of pions. Pions are spinless and couple to the magnetic field only via their angular momentum. This coupling gives rise to a Landau-type diamagnetism, i.e. $\chi^r < 0$.

In fact, the condensate of non-interacting point-like pions is expected to be superconducting and, as a result, a perfect diamagnet, which expels the magnetic field completely. This is demonstrated by explicit calculation in App. A. In full QCD, pions are not point-like free particles but interacting composite objects. This interaction poses an upper limit both on the density and on the conductivity. As a result, the magnetic susceptibility remains below its free-case value. In addition, unlike the chemical potential for free pions, the isospin chemical

potential in QCD is not bounded by the pion mass. For $\mu_I > m_\pi/2$, the density and the susceptibility are again influenced predominantly by QCD interactions. In particular, the rise of the Polyakov loop, Eq. (10) – as shown in the lower panel of Fig. 2 – reveals that deconfinement and the enhancement of n_I occur roughly simultaneously. This also implies that the pionic description breaks down. On the same figure, the susceptibility is also plotted as function of the isospin density, showing a linear section at low n_I and a saturation to about $\chi^r = -0.1$ as the density increases.

For even higher chemical potentials, QCD asymptotic freedom allows to neglect the strong interactions completely. Then, the magnetic susceptibility can be calculated for free quarks, giving [18]

$$\chi^r \xrightarrow{\mu_I \rightarrow \infty} \frac{1}{4\pi^2} \sum_f (q_f/e)^2 \cdot \log(\mu_I^2/\Lambda^2) > 0, \quad (14)$$

where the prefactor is related to the QED β -function and Λ is a dimensionful scale (in the on-shell renormalization scheme of the free theory, $\Lambda = m$) [13]. Thus, the susceptibility must eventually turn positive as μ_I increases. To explore the region where χ^r crosses zero, further simulations on finer lattices are necessary.

4. INTERPRETATION

Let us discuss the strong diamagnetic response above $\mu_I = m_\pi/2$ from a different point of view and consider how the charged pion mass responds to the magnetic field. Taking the pion as a point-like (relativistic) particle, the leading-order dependence reads

$$m_\pi(B) = \sqrt{m_\pi^2(0) + eB}, \quad (15)$$

as a consequence of the lowest-Landau-level structure for a scalar particle. Note that Eq. (15) is subject to corrections due to the B -dependence of the pion self-energy. These corrections are, however, small compared to the leading behavior [19]. Indeed, recent lattice QCD results [20] have confirmed Eq. (15) up to $eB \approx 0.4 \text{ GeV}^2$. At $T = 0$, the renormalized free energy can be calculated as the integral of the isospin density,

$$-\frac{\mathcal{F}(B, \mu_I)}{V} = \int_0^{\mu_I} d\mu'_I n_I(B, \mu'_I). \quad (16)$$

For $B = 0$, taking into account the dependence $n_I(\mu_I)$ from Fig. 1 (for $\lambda \rightarrow 0$), this implies that $-\mathcal{F}$ is zero up to $m_\pi/2$ and becomes positive above the threshold. Let us now switch on a weak magnetic field and consider the free energy up to $\mathcal{O}(B^2)$. To this order, $\mathcal{F}(B, \mu_I)$ still vanishes for chemical potentials up to the corresponding pion mass. However, due to Eq. (15), the Silver Blaze region expands as B grows. This can only be maintained if the surface $-\mathcal{F}$ has a large negative curvature in the B -

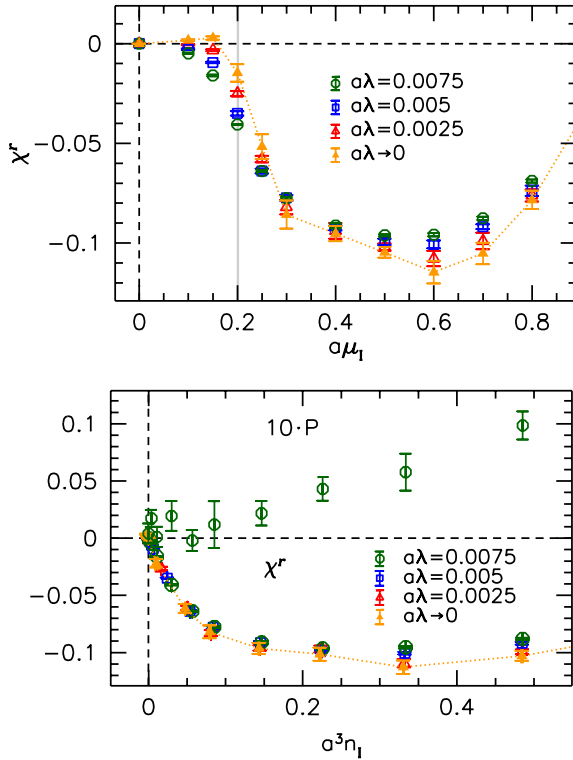


FIG. 2: Renormalized magnetic susceptibility as function of μ_I (upper panel) and of n_I (lower panel) for various values of λ (red, blue and green points), and the $\lambda \rightarrow 0$ extrapolations (yellow points), connected by the dotted line to guide the eye. The gray vertical line in the upper panel marks the onset of pion condensation. On the lower panel, the Polyakov loop for $a\lambda = 0.0075$ is also included.

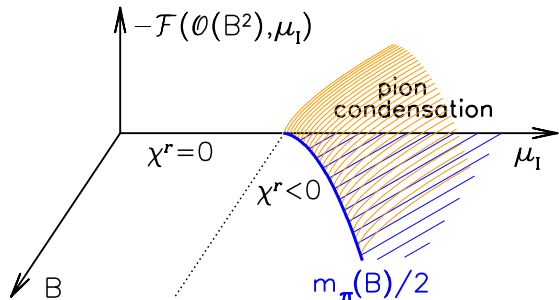


FIG. 3: Illustration of the negative of the free energy as a function of B and μ_I for small magnetic fields. The Silver Blaze region $\mathcal{F} = 0$ expands as B grows, implying a large negative magnetic susceptibility in the pion condensation phase.

direction, i.e., through a large negative susceptibility (for an illustration see Fig. 3). Thus, the pion condensation phase must exhibit strong diamagnetism – in line with our results presented in Sec. 3.

Note that the key component in the above argumentation was the scalar nature of the pion, which allowed for a phase with Bose-Einstein condensation and, at the same time, implied an increase in the mass as B grows, Eq. (15). For the baryonic chemical potential μ_B , the excited particles are protons and neutrons. In this case the baryon density grows much slower $n_B \propto (\mu_B^2 - m_B^2)^{3/2}$, and condensation can only occur via Cooper-pairing if the ground state is in the superfluid phase. Moreover, in the spin-half channel, the mass (to leading order) is independent of the magnetic field (both for neutrons and for protons), implying that the Silver Blaze region is also insensitive to B . Thus, χ^r is expected to be suppressed

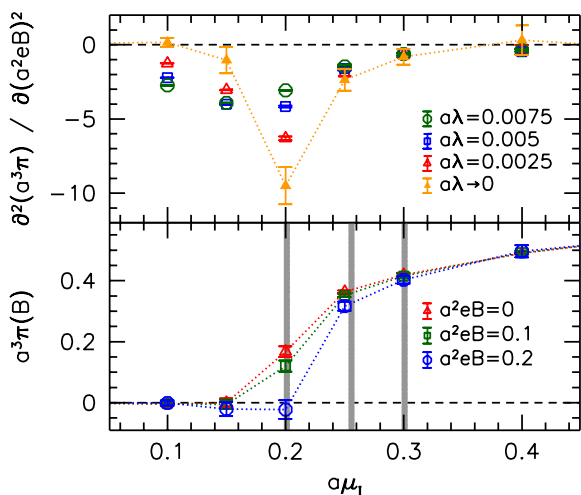


FIG. 4: Second derivative of the pion condensate (upper panel; the symbols are the same as in Fig. 2) and the $\lambda \rightarrow 0$ limit of the pion condensate at nonzero magnetic fields using the leading Taylor-expansion (lower panel). The gray vertical lines indicate the pion mass for each magnetic field (increasing from left to right).

for μ_B just above m_B . Note that in nature nucleons have anomalous magnetic moments that induce a dependence of the mass on B , and through that a nonzero value for χ^r , but due to the absence of direct condensation and due to the larger mass, these effects are not expected to produce a pronounced behavior like the one seen in Fig. 2.

To back up the picture described above, we also determined the lowest-order expansion coefficients of the observables in Eq. (8). In Fig. 4 we show the second derivative of the pion condensate with respect to eB and the reconstructed observable $\pi(B)$ for a few values of the magnetic field. As $\lambda \rightarrow 0$, the derivative is found to exhibit a pronounced dip around $\mu_I = m_\pi/2$ and, as a consequence, the rise in π is shifted to higher isospin chemical potentials as B is increased. The lattice data for the scalar condensate and for the isospin density show similar trends. Therefore, the results are in qualitative agreement with the discussion above, namely that the magnetic field shifts the onset of pion condensation to higher isospin chemical potentials. On the quantitative level, the results in the lower panel of Fig. 4 suggest that this shift is less pronounced than the expectation based on Eq. (15). (Note that the Taylor-expansion in B breaks down at the phase transition, where \mathcal{F} is non-analytic. Still, the reconstruction of $\pi(B)$ is expected to converge outside of the close vicinity of the onset isospin chemical potential.)

5. IMPLICATION FOR MAGNETARS

Next, we consider a possible implication of the diamagnetic pion condensed phase on the physics of strongly magnetized neutron stars. Charged pion condensation in neutron star cores has been the subject of discussion for a long time [21], as it is expected to have significant implications for, e.g., the equation of state [22] as well as neutron star cooling rates [23]. Assuming charge neutrality, together with equilibrium for neutron β -decay and for the process $n \rightarrow p + \pi^-$, the threshold density for pion condensation was found to be at a few times nuclear matter density (see, e.g., Ref. [22, 23]). The possibility of charged pion condensation and its consequences for neutron star physics have also been discussed more recently in, e.g., Refs. [24–26].

The most probable constituents of the pion condensed core are neutrons, protons, negatively charged pions, electrons and muons [27]. As we argued in Sec. 4, pions are strongly diamagnetic, whereas the contribution of protons and neutrons to χ^r is expected to be much smaller in magnitude. We remark that for the electron – in contrast to the other particles – the typical neutron star core magnetic fields exceed the rest mass squared (in fact, by several orders of magnitude). Thus, for the effect considered below, the electron contribution to the susceptibility is to be calculated in the strong field regime and not at $B = 0$. Another comment about the electron con-

tribution is in order here. The free energy in the presence of magnetic fields contains a thermal/dense contribution at nonzero T and/or μ , as well as a vacuum term that stems from virtual particles at $T = \mu = 0$ and that dominates in the strong field regime $eB \gg T^2, \mu^2, m^2$ [18]. However, as we will see, the vacuum term has no effect on the mechanism discussed below. The thermal/dense contribution to χ^r has been calculated several times in the literature [18, 28–30] and was always found to be below a few percents for the magnetic field strengths considered here $B \approx 10^{18}$ G. Similarly small estimates for the muon, proton and neutron contributions were also given in Ref. [30]. Altogether we can thus estimate the total magnetic susceptibility in the magnetar core by the pionic contribution and take $\chi^r \approx -0.1$ as a typical value that we obtained.

The proposed mechanism involves a gradient force that emerges in inhomogeneous magnetic fields. Namely, the minimization of the free energy induces the force density,

$$f_d = -\frac{1}{V} \nabla \mathcal{F} = \chi^r |eB| |\nabla |eB|. \quad (17)$$

Note that this force is only sensitive to the magnetic properties of the medium, and neither the energy $B^2/2$ of the magnetic field, nor the above mentioned vacuum contribution in \mathcal{F} contributes to f_d (assuming that B is constant in time, i.e. there is no feedback from matter to the magnetic field configuration). Note moreover that since the free energy is a Lorentz-scalar, f_d only depends on the magnitude of B . We adopt the poloidal magnetic field profile $\mathbf{B}(r, \theta)$ of Ref. [7] for a rotating magnetar with radius $R = 10$ km and central field strength $1.5 \cdot 10^{18}$ G. The rotation axis is given by $\theta = 0$. Inserting $\chi^r \approx -0.1$ for the susceptibility we obtain $f_d(r)$, see the curves in Fig. 5 for three fixed values of the polar angle θ .

The so obtained force density is to be compared to the gradient of the isotropic pressure profile $p(r)$ in the star. For a first approximation, we take the simplified case of a star with constant density (see Eq. (3.157) of

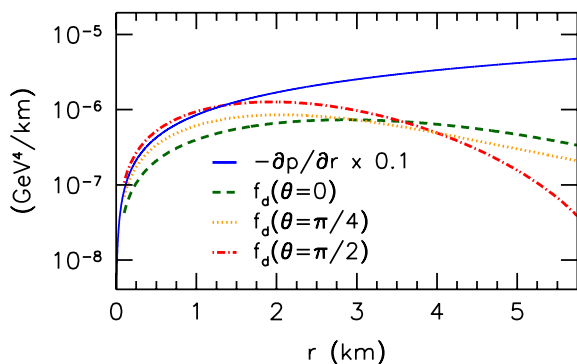


FIG. 5: The force generated by QCD diamagnetism (along various directions specified by the polar angle θ) and 10% of the pressure gradient as functions of the radial coordinate.

Ref. [27]), and consider typical values for the central pressure $p_c \approx 10^{34}$ Pa. The resulting gradient is also included in Fig. 5, indicating that in this case the diamagnetic effect amounts to up to 10% of the gravitational pressure gradient in the inner core $r \lesssim 3$ km. The curves for $f_d(r, \theta)$ also reveal that the diamagnetic force is anisotropic and tends to push material from the center towards the equator. Thus, we expect that the diamagnetism of isospin-asymmetric QCD matter plays a relevant role for the description of convective processes in the inner core. We mention that a similar mechanism in the case of heavy-ion collisions was discussed in Ref. [31].

6. CONCLUSIONS

We have discussed the QCD phase diagram in the $\mu_I - B$ plane for the first time using lattice simulations. This setup has a complex action problem, which was circumvented through a Taylor-expansion in B at nonzero isospin chemical potentials. We measured thermodynamic observables for a wide range of μ_I values, in the Silver Blaze region, through the onset of pion condensation at $\mu_I = m_\pi/2$, up to lattice saturation. The results indicate that the condensation threshold is shifted to higher values of μ_I as B grows, in qualitative agreement with the dependence $m_\pi(B)$ of the pion mass on the magnetic field. We demonstrated how this tendency explains the observed strong diamagnetic behavior of the system in the pion condensation phase. The diamagnetic nature of the pion condensate is also predicted by free-case arguments, see the analytic calculation of the pionic susceptibility in App. A.

In addition, we also presented an argument suggesting that the magnetic response of the QCD ground state is most sensitive to isospin chemical potentials, and the baryon chemical potential is not expected to play a dominant role in this respect. Our results were obtained on coarse lattices with a larger-than-physical pion mass, and thus should be considered exploratory. However, since the findings are understood in terms of general arguments like the existence of a pion condensation phase and the diamagnetic nature of pions, the results are not expected to change qualitatively if the physical point and the continuum limit are approached.

We conclude by sketching the magnetic nature of QCD matter on the $T - \mu_I$ phase diagram. At $\mu_I = 0$, lattice simulations have shown that the susceptibility is positive for $T \gtrsim 120$ MeV [12, 13, 31–33], whereas it becomes slightly negative for lower temperatures [13]. The latter diamagnetic region is predicted by χ PT and by the Hadron Resonance Gas model [13, 33], and also stems from the presence of charged pions. However, while at $T = 0$ and $\mu_I > m_\pi/2$, pions are created in abundance, at $T > 0$ they are induced merely by thermal fluctuations. Accordingly, the diamagnetic response at $0 < T \lesssim 120$ MeV is much weaker ($\chi^r \approx -0.002$ [13]) than the one in the pion condensation phase ($\chi^r \approx -0.1$).

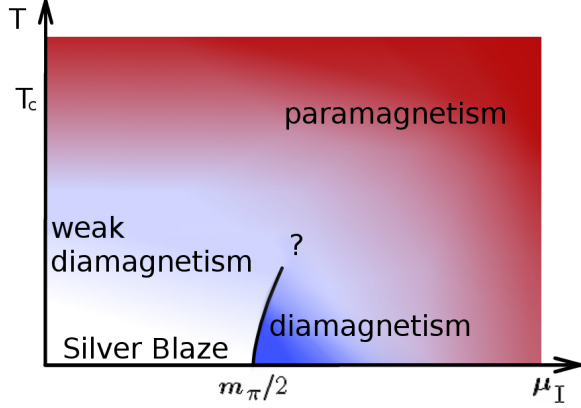


FIG. 6: Conjecture of the magnetic structure of the phase diagram in the $T-\mu_I$ plane. Regions with positive (negative) susceptibilities are represented by red (blue) and darker colors mark larger magnitudes. At $\mu_I = 0$ the transition from diamagnetism to paramagnetism occurs slightly below the chiral crossover temperature $T_c \approx 150$ MeV [13]. The solid line at high μ_I represents a true phase transition separating the vacuum and the pion condensation phase. There may be additional phase transition lines in the interior of the diagram, indicated by the question mark.

Note also that around the deconfinement temperature ($T_c \approx 150$ MeV) at $\mu_I = 0$, the susceptibility was found to be significantly smaller ($\chi^r \approx 0.01$ [13]) than the magnitude of our results in the pion condensed phase. Well above the deconfinement transition temperature at $\mu_I = 0$, the dominant degrees of freedom are quarks, giving rise to strong paramagnetism, with $\chi^r \propto \log(T)$, similarly as in Eq. (14), just with μ_I replaced by T [13]. Thus, asymptotic freedom in QCD ensures that QCD matter is paramagnetic for very high values of T and/or μ_I .

Based on this picture, our conjecture of the magnetic phase diagram – summarizing the dia- and paramagnetic regions of QCD matter – is shown in Fig. 6. The phase transition at $\mu_I = m_\pi/2$ is expected to bend to the right [16] and either persist towards higher temperatures or end at the deconfinement phase transition line if the latter exists. Which scenario is the case and whether there are additional phase transition lines in the diagram is presently unclear. The isospin density has been shown to change the nature of the chiral transition in 8-flavor QCD [34]. The structure of the $T - \mu_I$ phase diagram has been studied in various model frameworks as well [35–38]. A possible critical endpoint at nonzero isospin densities and magnetic fields was also discussed in Refs. [39, 40] in model setups. To determine the detailed structure of the interior of the phase diagram on the lattice for the interesting case of 2 or 2+1 flavors, further simulations are necessary.

Acknowledgements. This work was supported by the DFG (SFB/TRR 55) and by the Alexander von Humboldt Foundation. The author thanks Gert Aarts, Mas-

simo D’Elia, Kim Splittorff and Laurence Yaffe for useful discussions, and Gunnar Bali, Falk Bruckmann, Andreas Schäfer for a careful reading of the manuscript.

Appendix A: Susceptibility of free pions

In this appendix we calculate the magnetic susceptibility of free non-relativistic pions. Since we aim to describe the condensation phase at low temperatures, where only one species – say, the π^- – contributes, we consider a pion with charge $q = -e$ and exclude its positively charged antiparticle for simplicity. The energy levels read

$$E_n = m_\pi + \frac{|qB|}{2m_\pi}(2n+1) + \frac{p_z^2}{2m_\pi}, \quad (\text{A1})$$

where p_z is the momentum parallel to B , and we included the rest mass m_π of the pion in the energy. The matter contribution to the free energy of the pion gas at temperature T and chemical potential μ_π in a finite volume V is written as

$$\mathcal{F}^m = \frac{|qB| \cdot V}{4\pi^2} \int dp_z \sum_n T \log \left[1 - e^{-(E_n - \mu_\pi)/T} \right]. \quad (\text{A2})$$

This expression does not contain the vacuum contribution, which stems from virtual pions at $\mu_\pi = T = 0$ in the presence of the magnetic field (see, e.g., Refs. [18, 41]). However, the vacuum part does not contribute to the renormalized susceptibility at $B = 0$, nor does it have an effect on the mechanism discussed in Sec. 5. It is therefore neglected in the following.

The renormalized susceptibility is obtained as the second derivative of \mathcal{F}^m with respect to eB . Since the sum and the integral in \mathcal{F}^m are ultraviolet finite, these can be interchanged with the derivative,

$$\chi^r = \frac{1}{4\pi^2} \int dp_z \sum_n \frac{(2n+1)/m_\pi}{1 - \exp\left(\frac{p_z^2}{2m_\pi T} - \frac{\mu_\pi - m_\pi}{T}\right)}. \quad (\text{A3})$$

The sum over n is calculated using ζ -function regularization, while the integral gives a polylogarithm function,

$$\chi^r = \frac{-1}{12\pi^2} \frac{\sqrt{2\pi T}}{\sqrt{m_\pi}} \cdot \text{Li}_{1/2}[e^{(\mu_\pi - m_\pi)/T}]. \quad (\text{A4})$$

Note that for our bosonic system, the chemical potential cannot exceed m_π . In the Silver Blaze region $\mu_\pi < m_\pi$, the zero-temperature limit of the polylogarithm function vanishes, resulting in $\chi^r = 0$. However, for $\mu_\pi \rightarrow m_\pi$ the susceptibility diverges for any infinitesimally small temperature,

$$\lim_{T \rightarrow 0} \chi^r(\mu_\pi < m_\pi) = 0, \quad \lim_{\mu_\pi \rightarrow m_\pi} \chi^r(T > 0) = -\infty. \quad (\text{A5})$$

We remark that if the condensation phase is approached by gradually lowering the temperature at fixed density n ,

pions start to condense at the critical temperature [42]

$$T_c = \frac{2\pi}{m_\pi} \left(\frac{n}{\zeta(3/2)} \right)^{2/3}, \quad (\text{A6})$$

which is always non-vanishing.

A remark about χ^r approaching $-\infty$ is in order. Notice that B equals the magnetic field acting in the medium, which is to be distinguished from the external magnetic field H that would be present in the absence of pions. The two fields are connected by the magnetization,

$$B = H + \mathcal{M}e, \quad \mathcal{M} = -\frac{1}{V} \frac{\partial \mathcal{F}^m}{\partial (eB)}. \quad (\text{A7})$$

For weak fields, $\mathcal{M} = \chi^r \cdot (eB)$, which allows to express the magnetic permeability p_m of the medium as

$$p_m \equiv \frac{B}{H} = \frac{1}{1 - e^2 \chi^r}. \quad (\text{A8})$$

Clearly, for $\chi^r \ll 1$ the difference between B and H is negligible and p_m is very close to unity. However, for $\chi^r \rightarrow -\infty$, the permeability vanishes, signalling that the magnetic field is expelled from the system completely. This perfect diamagnetism is characteristic for superconductors. Indeed, at $\mu_\pi = m_\pi$ the system becomes superconducting due to the condensation of charged pions.

-
- [1] R. C. Duncan and C. Thompson *Astrophys. J.* **392** (1992) L9.
 - [2] C. Thompson and R. C. Duncan *Astrophys. J.* **473** (1996) 322.
 - [3] C. Cutler *Phys.Rev.* **D66** (2002) 084025, [[gr-qc/0206051](#)].
 - [4] D. Price and S. Rosswog *Science* **312** (2006) 719–22, [[astro-ph/0603845](#)].
 - [5] M. Anderson, E. W. Hirschmann, L. Lehner, S. L. Liebling, P. M. Motl, *et. al.* *Phys.Rev.Lett.* **100** (2008) 191101, [[arXiv:0801.4387](#)].
 - [6] A. K. Harding and D. Lai *Rept.Prog.Phys.* **69** (2006) 2631, [[astro-ph/0606674](#)].
 - [7] M. Bocquet, S. Bonazzola, E. Gourgoulhon, and J. Novak *Astron.Astrophys.* **301** (1995) 757, [[gr-qc/9503044](#)].
 - [8] J. Kogut and D. Sinclair *Phys.Rev.* **D66** (2002) 034505, [[hep-lat/0202028](#)].
 - [9] M. Lüscher *JHEP* **1008** (2010) 071, [[arXiv:1006.4518](#)].
 - [10] S. Borsányi, S. Dürr, Z. Fodor, C. Hoelbling, S. D. Katz, *et. al.* *JHEP* **1209** (2012) 010, [[arXiv:1203.4469](#)].
 - [11] G. 't Hooft *Nucl. Phys.* **B153** (1979) 141.
 - [12] L. Levkova and C. DeTar *Phys.Rev.Lett.* **112** (2014) 012002, [[arXiv:1309.1142](#)].
 - [13] G. Bali, F. Bruckmann, G. Endrődi, S. Katz, and A. Schäfer *JHEP* **1408** (2014) 177, [[arXiv:1406.0269](#)].
 - [14] J. S. Schwinger *Phys.Rev.* **82** (1951) 664–679.
 - [15] K. Splittorff, D. Toublan, and J. Verbaarschot *Nucl.Phys.* **B639** (2002) 524–548, [[hep-ph/0204076](#)].
 - [16] D. Son and M. A. Stephanov *Phys.Rev.Lett.* **86** (2001) 592–595, [[hep-ph/0005225](#)].
 - [17] J. Kogut, M. A. Stephanov, D. Toublan, J. Verbaarschot, and A. Zhitnitsky *Nucl.Phys.* **B582** (2000) 477–513, [[hep-ph/0001171](#)].
 - [18] P. Elmfors, D. Persson, and B.-S. Skagerstam *Astropart.Phys.* **2** (1994) 299–326, [[hep-ph/9312226](#)].
 - [19] G. Colucci, E. Fraga, and A. Sedrakian *Phys.Lett.* **B728** (2014) 19–24, [[arXiv:1310.3742](#)].
 - [20] G. Bali, F. Bruckmann, G. Endrődi, Z. Fodor, S. Katz, *et. al.* *JHEP* **1202** (2012) 044, [[arXiv:1111.4956](#)].
 - [21] A. B. Migdal, E. Saperstein, M. Troitsky, and D. Voskresensky *Phys.Rept.* **192** (1990) 179–437.
 - [22] I.-S. Suh and G. Mathews *Astrophys.J.* **546** (2001) 1126–1136, [[astro-ph/9912301](#)].
 - [23] O. Maxwell, G. Brown, D. Campbell, R. Dashen, and J. Manassah *Astrophys.J.* **216** (1977) 77–85.
 - [24] T. Takatsuka and R. Tamagaki *Prog.Theor.Phys.Suppl.* **112** (1993) 107–122.
 - [25] K. Takahashi *Prog.Theor.Phys.* **108** (2002) 689–701.
 - [26] A. Ohnishi, D. Jido, T. Sekihara, and K. Tsubakihara *Phys.Rev.* **C80** (2009) 038202, [[arXiv:0810.3531](#)].
 - [27] N. Glendenning, *Compact Stars: Nuclear Physics, Particle Physics, and General Relativity*. Second edition. Springer New York, 2000.
 - [28] R. Blandford and L. Hernquist *J. Phys* **C15** (1982) 6233.
 - [29] P. Elmfors, P. Liljenberg, D. Persson, and B.-S. Skagerstam *Phys.Rev.* **D51** (1995) 5885–5888, [[hep-ph/9407356](#)].
 - [30] J. Dong, W. Zuo, and J. Gu *Phys.Rev.* **D87** (2013) 103010, [[arXiv:1305.4533](#)].
 - [31] G. Bali, F. Bruckmann, G. Endrődi, and A. Schäfer *Phys.Rev.Lett.* **112** (2014) 042301, [[arXiv:1311.2559](#)].
 - [32] C. Bonati, M. D’Elia, M. Mariti, F. Negro, and F. Sanfilippo *Phys.Rev.Lett.* **111** (2013) 182001, [[arXiv:1307.8063](#)].
 - [33] C. Bonati, M. D’Elia, M. Mariti, F. Negro, and F. Sanfilippo *Phys.Rev.* **D89** (2014) 054506, [[arXiv:1310.8656](#)].
 - [34] P. de Forcrand, M. A. Stephanov, and U. Wenger *PoS LAT2007* (2007) 237, [[arXiv:0711.0023](#)].
 - [35] Z. Zhang and Y.-X. Liu *Phys.Rev.* **C75** (2007) 064910, [[hep-ph/0610221](#)].
 - [36] T. Sasaki, Y. Sakai, H. Kouno, and M. Yahiro *Phys.Rev.* **D82** (2010) 116004, [[arXiv:1005.0910](#)].
 - [37] K. Kamikado, N. Strodthoff, L. von Smekal, and J. Wambach *Phys.Lett.* **B718** (2013) 1044–1053, [[arXiv:1207.0400](#)].
 - [38] R. Stiele, E. S. Fraga, and J. Schaffner-Bielich *Phys.Lett.* **B729** (2014) 72–78, [[arXiv:1307.2851](#)].
 - [39] X. Kang, M. Jin, J. Xiong, and J. Li [[arXiv:1310.3012](#)].
 - [40] P. Costa, M. Ferreira, H. Hansen, D. P. Menezes, and C. Providência *Phys.Rev.* **D89** (2014) 056013, [[arXiv:1307.7894](#)].
 - [41] G. Endrődi *JHEP* **1304** (2013) 023, [[arXiv:1301.1307](#)].
 - [42] J. Kapusta and C. Gale, *Finite-Temperature Field Theory: Principles and Applications*. Cambridge monographs on mechanics and applied mathematics. Cambridge University Press, 2006.